ASME Journal of Engineering for Gas Turbines and Power
Online journal at:
https://asmedigitalcollection.asme.org/gasturbinespower

A Modified Loss Breakdown Approach for Axial Turbines Operating With Blended Supercritical Carbon Dioxide

Abdelrahman S. Abdeldayem
Thermo-Fluids Research Centre,
School of Science & Technology, City,
University of London,
Northampton Square,
London EC1V 0HB, UK

Salma I. Salah
Thermo-Fluids Research Centre,
School of Science & Technology, City,
University of London,
Northampton Square,
London EC1V 0HB, UK

Martin T. White
Thermo-Fluids Research Centre,
School of Science & Technology, City,
University of London,
Northampton Square,
London EC1V 0HB, UK;
Thermo-Fluid Mechanics Research Centre,
School of Engineering and Informatics,
University of Sussex,
Brighton BN1 9RH, UK

Abdulnaser I. Sayma
Thermo-Fluids Research Centre,
School of Science & Technology, City,
University of London,
Northampton Square,
London EC1V 0HB, UK

In this paper, a modified loss breakdown approach is introduced for axial turbines operating with supercritical carbon dioxide (sCO_2) mixtures using computational fluid dynamics (CFD) results. Loss breakdown analysis has been previously developed using two approaches, however each approach has its own uncertainties. The first approach neglects the effects of the cross-interaction between the different loss sources, while the second approach ignores the potential changes to the boundary layer thicknesses and the loss source domains. Although the second methodology accounts for the interactions between the different loss sources, it may produce less accurate predictions for compact machines like sCO_2 turbines where the boundary layer may dominate the flow passage. The proposed methodology aims to obtain the turbine loss breakdown using a single CFD model where all sources of aerodynamic loss coexist, while considering variable loss regions defined based on the velocity and entropy distribution results. A steady-state, single-stage, single-passage, three-dimensional numerical model is setup to simulate the turbine and verify the loss audit methodology. The results are verified against the published loss audit methodologies for a 130 MW axial turbine operating with CO_2/C_6F_6 blend, designed using an in-house mean line design code. The results show a good agreement between the proposed approach and the multiple-model approaches from the literature. However, the existing approaches appear to overestimate endwall losses by 13–16% and underestimate the profile losses by 11–31% compared to the proposed approach. Compared to the Aungier mean line loss model, large differences in loss sources are observed from the CFD results, especially for the stator and rotor endwall losses which are found to be 3.2 and 1.6 times the CFD values, respectively. This helps to indicate limitations in existing mean line loss models.
[DOI: 10.1115/1.4062478]

Keywords: axial turbine, CFD, loss audit, aerodynamic losses, sCO_2 blends

1 Introduction

Power cycles based on supercritical carbon dioxide (sCO_2), and sCO_2 blends, have been proposed as promising candidates to increase the efficiency of concentrated-solar power (CSP) power blocks, and are being considered for next generation CSP plants [1]. Owing to the thermodynamic properties of CO_2, and CO_2 blends, sCO_2 turbines are characterized by a small machine size due to the high density of the working fluid and the low pressure ratios of the cycle. This leads to compact machines, with potentially lower installation costs [2]. However, the design of sCO_2 turbines poses interesting design challenges associated with the compact turbine design, the high density and low kinematic viscosity of the working fluid [3]. Improving the performance of turbomachinery components is therefore a key aspect in realizing a successful power plant design to achieve the highest possible cycle efficiency and in order to minimize the levelized cost of electricity (LCOE). In this respect, understanding and being able to quantify sources of aerodynamic loss within axial turbines provides an important means to attain the best power cycle performance.

Principally, turbine design and performance analyses take place through multiple sequential phases starting with preliminary aerodynamic turbine design and optimization, followed by three-dimensional (3D) blade geometry generation, aerodynamic analysis using computational fluid dynamics (CFD) and finally, blade shape optimization based on the 3D numerical model results [4]. The available mean line design loss models are developed and calibrated for traditional working fluids (i.e., steam and air [5–8]) and therefore they may introduce uncertainty into the design process. Therefore, obtaining the loss breakdown using numerical models is important to better understand the aerodynamic behavior of turbines operating with sCO_2 and sCO_2 blends and to provide an assessment of existing mean line methods.

Axial turbines are characterized by numerous aerodynamic loss sources such as tip clearance, secondary flow, endwall, profile, trailing edge, incidence, partial admission, shock wave, and mixing losses. According to Langston [9], secondary flow losses are defined

Manuscript received November 8, 2022; final manuscript received April 10, 2023; published online July 11, 2023. Assoc. Editor: Phillip Ligrani.

as undesired flow streams causing turbulence and vortices which increase the stage pressure loss. Endwall and profile losses are similar to secondary flow losses, but originate from the boundary layers that develop on the endwalls and blade walls, respectively. Tip clearance leakage is critical, especially in high reaction stages because the pressure difference across rotor blades can be significant [10]. Additionally, tip leakage induces vortices that interact with the secondary flow downstream the blades. The trailing edge losses, also called mixing loss [11], are formed due to the sudden change in the flow passage area in the streamwise direction downstream of the trailing edge. Denton and Xu [12] suggested that the trailing edge loss is minor and can be neglected in subsonic flows, although it increases significantly as the flow becomes supersonic.

Numerous studies have focused on introducing and implementing techniques to estimate aerodynamic loss breakdown using CFD simulations for different working fluids like air, sCO_2 and organic fluids. To express the magnitude of different aerodynamic losses, the entropy increase (Δs) is commonly used. One of these approaches is based on defining the axial distribution of mass averaged entropy from inlet to outlet and attributing different intervals along the streamwise location to different loss sources [13]. Another approach evaluates the change in entropy across the turbine stage by the elimination of one, or more, loss sources using a set of sequential CFD simulations [14]. Yoon et al. [14] applied this method to the loss audit analysis of an axial gas turbine stage where the working fluid was modeled as an ideal gas. It has been found that the trailing edge losses are dominant, accounting for more than one-third of the total aerodynamic losses. In comparison, De-Servi et al. [11], Keep and Jahn [15], and Wheeler and Ong [13] evaluated the loss breakdown of radial-inflow turbines operating with the siloxane MM, sCO_2, and *n*-pentane, respectively. However, these models neglect the interaction between different sources of loss when one or more loss sources are eliminated from the simulations. Further details related to these techniques are described in Sec. 2.1.

Entropy generation rate is another approach introduced by Pullan et al. [16] to represent the energy generated from each domain element per unit volume per degree of temperature change (W/m^3K). This indicates where and how much entropy is generated within the flow domain. This technique has been used to evaluate the aerodynamic losses from a single numerical model by dividing the flow domain into eight arbitrary regions selected to show the losses generated due to the hub surface, tip gap, upstream domain, downstream domain, blade suction side surface, blade pressure side surface, passage domain, and blade trailing edge domain. Although the resulting loss structure is defined by region, instead of the common loss definition by source, this approach was found to be satisfactory in the proposed study because the use of this tool was limited to comparing the results of different nozzle guide vane (NGV) designs to assess their performance. Similarly, Newton et al. [17] considered an arbitrary area division of the turbine flow passage, where the rotor was divided into seven volumes and the entropy generation technique was applied to evaluate the loss breakdown by region. The resulting loss breakdown structure was used to assess the performance of a radial-inflow turbine at full and partial admission and the results were compared to show dominant loss regions in each case.

Denton and Pullan [18] proposed an enhancement to the technique of loss breakdown introduced by Pullan et al. [16] and applied it to a gas turbine. In this approach, they tracked changes in the boundary layers to investigate the sources of endwall loss in axial flow turbines. Within that study, it was proposed that the loss breakdown can be obtained by dividing the flow domain into regions and tracking vortices originating from the endwalls and defining an arbitrary offset of 5% of the span from the endwalls to express the endwall losses. The entropy generation is then integrated over the defined volumes to represent the loss contribution from each region. Later, Newton et al. [19] applied a similar technique to an air turbine where it was found that this methodology is useful in determining the areas that contribute more to aerodynamic losses.

Although the methodology introduced by Newton et al. [19] depends on a single numerical model where all sources of loss coexist, the assumed loss definition domains are fixed and need to be calibrated for each case study individually. This means the loss domains that have been selected for the proposed air turbine case study would not be suitable for other machines operating with different Reynolds number or different working fluids. In the current study, an improved methodology is presented to quantify the loss breakdown using a single CFD model where all sources of aerodynamic losses coexist. In the proposed methodology, the contours defining each loss source are selected based on the velocity and entropy distributions on a set of selected planes, instead of defining fixed loss domains. This makes the proposed methodology suitable for different types of flow regimes and different working fluids, which includes sCO_2 machines which are characterized by compact designs.

In this paper, aerodynamic loss breakdown approach is introduced for large-scale axial turbines operating with sCO_2 based mixtures, which are intended for concentrated solar power (CSP) applications. This methodology aims to improve the current methodologies in order to overcome their weaknesses, whilst also assessing for the first time aerodynamic losses in sCO_2 turbines. The loss audit methodologies previously introduced within the literature are first reviewed in Sec. 2.1 which is followed by a detailed description of the proposed methodology in Sec. 2.2. The model verification is discussed in Sec. 3, which considers an air turbine case study from the literature. Finally, results and discussions are presented in Sec. 4; where a detailed comparison between the loss breakdown approaches is discussed and a sensitivity study is carried out for the parameters involved in the new loss breakdown approach to assess its reliability and accuracy.

2 Numerical Loss Audit

The numerical model used in the current study is first described, including details of the mesh refinement study. This is followed by a review of the loss audit approaches previously published in the literature (Sec. 2.1), alongside the newly proposed loss audit methodology (Sec. 2.2).

The initial turbine flow path is generated using an in-house mean line design tool that has been previously published by the authors [20,21]. In this model, the steady-state mass, energy, and momentum equations are solved to obtain the blade geometry, velocity triangles and thermodynamic properties for all design stages. The mean line design process is initiated using a set of boundary conditions defined based on thermodynamic cycle analysis; this includes the inlet total temperature and pressure, pressure ratio, and mass flowrate. Alongside the boundary conditions, a set of decision variables are defined, which includes the flow coefficient, loading coefficient, degree of reaction, pitch to chord ratio, and tip clearance gap. Repeating stages are assumed, which means the flow angle and absolute velocity are approximately the same at the inlet to each stage.

To predict the turbine efficiency the Aungier loss model is used [7]. This model has been found to be the most suitable for sCO_2 turbines, and is integrated with the mean line tool to evaluate the performance of the produced turbine design as previously detailed in [21]. Multiple losses are considered within the Aungier loss model which include profile losses, secondary flow losses, tip clearance and trailing edge losses. This model has been previously verified against multiple cases from the literature operating over a wide range of working fluids that include air, and nonconventional working fluids such as sCO_2 [20,21]. The results of both verification cases indicate that the model is capable of predicting the turbine performance with a good accuracy margin where a maximum percentage differences in the total-to-total efficiency of 1.3% was found compared to the cases from the literature.

The resulting mean line flow path design is used as the basis for building the two-dimensional blade profiles and the 3D blade geometry in order to setup the numerical simulations as shown in Fig. 1. The stator and rotor blades look similar because the flow path considered in this paper is designed for a flow coefficient, loading

coefficient, and degree of reaction of 0.5, 1.0, and 0. 5, respectively. This leads to symmetric velocity triangles at the inlet and outlet of each rotor blade. In addition, the pitch to chord ratio is assumed constant for both stator and rotor blades and the number of stator and rotor blades are very similar. This means the stator and rotor chord lengths are comparable. In the proposed design, untwisted turbine blades are assumed due to the relatively small blade height to mean diameter ratio, which is less than 4% for the longest blades which are found within the last stage.

The numerical model is a steady-state, 3D, viscous, multistage CFD model with a single stator and rotor domains modeled for each stage. As such, periodic boundary conditions in the circumferential direction for each stage are applied, as reported in Fig. 1. The solver used for the numerical simulation is ANSYS CFX 2020R2. The steady-state assumption is commonly used for turbomachinery applications, especially when the flow is subsonic where it is not expected to have shock waves extending across the rotor–stator interface, and the differences between steady-state and unsteady performance results are negligible [13,14]. The stator–rotor interface is modeled with a mixing plane interface, which is the most reliable approach in steady-state simulations that provides a reasonable level of accuracy [22]. The turbulence model is the k–ω SST model which has been reported to produce accurate predictions for turbomachinery flows [23]. The boundary conditions applied to this model are the inlet total pressure, inlet total temperature, and outlet static pressure, while the mass flowrate is calculated and then verified against the mean line design inputs. No tip clearance is assumed between the rotor blades and casing as the current study is focused on shrouded blades. Therefore, the blade shroud wall is modeled as a rotating surface.

Once the simulation is completed for the four-stages, the loss audit is carried out on the first and last stages to quantify the different loss sources and provide a comparison against the Aungier mean line loss model.

The fluid properties are evaluated using the Peng-Robinson equation of state, whilst the binary interaction parameter required to model the mixture, are obtained by fitting the equations of state to experimental data [24]. The properties are included within the CFD model using look-up tables that cover the expected pressure and temperature ranges. The selected pressure range is set to 10 and 300 bar to cover the full range of expected pressure values within the solution domain. Similarly, the temperature range is set between 400 and 1200 K. The resolution of the property tables is defined using the number of pressure and temperature divisions, where different table sizes were tested ranging between 200×200 and 700×700 points. It has been found that the variations in the model results are negligible when the table size is greater than 500×500.

A mesh sensitivity analysis is conducted to ensure a grid independent numerical solution, as reported in Fig. 2. This figure shows the total-to-total efficiency against the number of grid points. It can be seen that the variation in total-to-total efficiency is less than 0.05% for a mesh larger than 1.3 million grid points per stage, relative to the finest mesh. Furthermore, the mesh is refined near the blade, hub and shroud surfaces of both the stator and rotor domains to ensure $y^+ \approx 1$, such that the boundary layer development over the walls is accurately modeled. The obtained y^+ distribution and corresponding inlet flow conditions are reported in Fig. 3 and Table 1, respectively. The average y^+ values on the blade, hub, and shroud walls for both the stator and rotor are found between 0.40 and 0.77.

The mesh is constructed based on the first layer thickness on the walls, the growth rate, and the number of elements in the spanwise direction, which are varied to form the 4 different grid sizes, as indicated in Table 2. For the stator domain, the total number of grid points for the four meshes is 0.31×10^6, 0.70×10^6, 1.4×10^6, and 2.9×10^6, respectively. For each grid, the velocity and entropy distributions are reported at three different radial lines extending from the hub to shroud, where their locations are arbitrarily defined

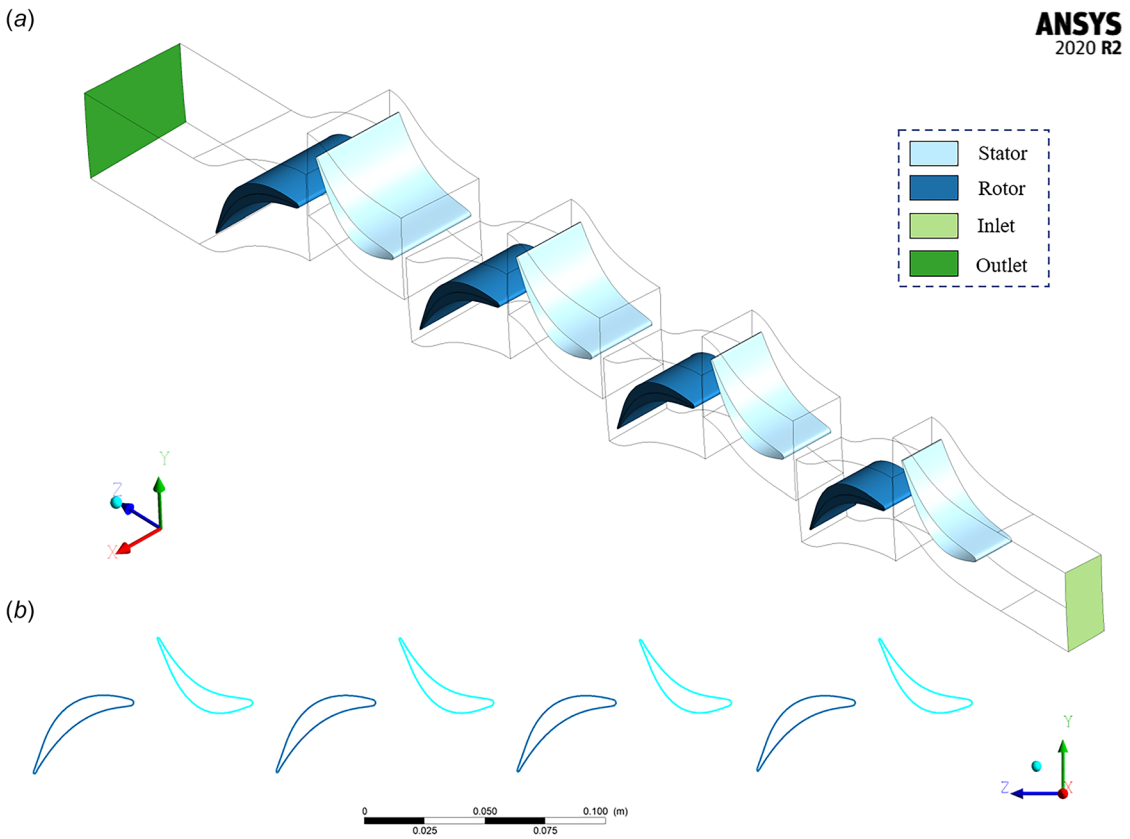

Fig. 1 3D geometry of the turbine numerical domain: (*a*) and a cross section of the blade profile (*b*) of the four-stage turbine model

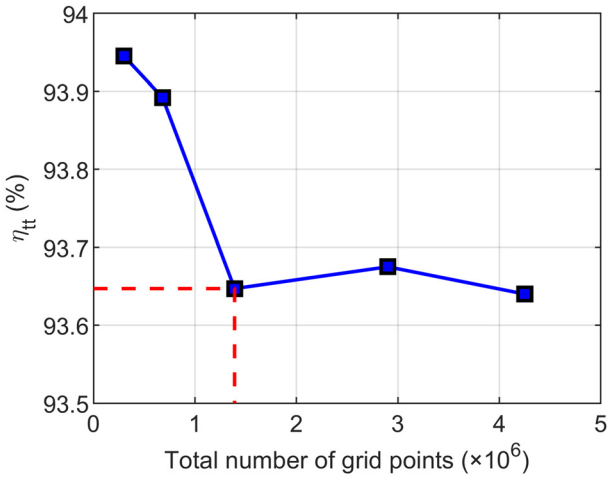

Fig. 2 Mesh sensitivity study for the first stage of the sCO_2-C_6F_6 4-stage design

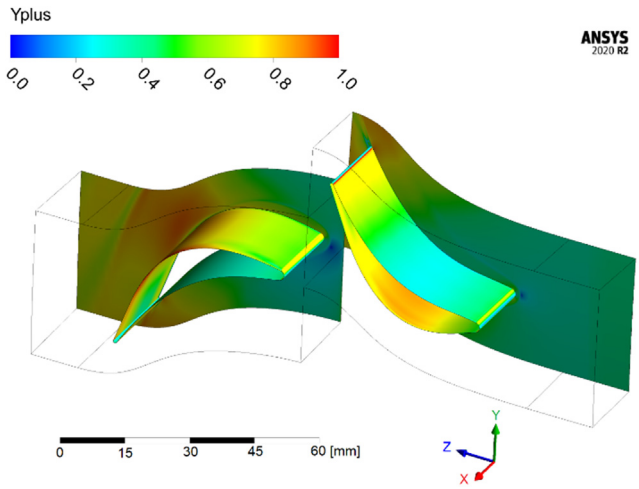

Fig. 3 y^+ distribution over the hub, and blade surfaces of the first stage of a 130 MW, four-stages, sCO_2-C_6F_6 design

Table 1 Calculated flow conditions at the turbine inlet/outlet boundaries

Parameter	Value
Inlet absolute velocity (m/s)	87.9
Inlet turbulence intensity (%)	5%
Inlet Mach number	0.50
Outlet Mach number	0.57
Inlet Reynold's number	1.2×10^7
Viscous boundary layer thickness approaching the stator leading edge (mm)	0.73

to represent different flow conditions along the solution domain. The first and second lines are selected at 70% of the stator and rotor chord length, and 5% away from the blade suction side surface. The third line is selected downstream of the rotor trailing edge at 5% of the chord length. The radial distributions of the velocity magnitude along the three lines are reported in Figs. 4(*a*)–4(*c*), while the entropy distributions are reported in Figs. 4(*d*)–4(*f*). It can be seen from the figures that slight differences appear between grid 1, 2, and 3, while the differences between grid 3 and grid 4 are negligible.

The main aerodynamic loss sources in a sCO_2 axial flow turbine operating at the design point are endwall, secondary flow, profile, trailing edge, and interface losses. Other aerodynamic losses such as shock, incidence and partial admission losses are less likely to happen because the turbine stage is entirely subsonic and running under design operating conditions. Tip clearance losses are not considered for this study as the proposed design assumes shrouded turbine blade. Endwall losses develop due to the viscous effect of the working fluid near the hub and shroud walls. Secondary flows are defined as undesired flow streams producing additional shear stresses between the fluid layers that increase entropy and decrease turbine efficiency. Denton and Pullan [18] have shown that secondary flows do not incur losses without interacting with the endwall boundary layers, as well as those on the blade suction side, and as such secondary flow and endwall losses can be aggregated and treated as a single loss source. Similar to endwall losses, profile losses develop around the blade wall due to the viscous effect. Trailing edge losses are generated due to the sudden expansion that occurs due to the increase in the flow path area near the blade trailing edge which causes a loss in total pressure and an increase in entropy. The interface loss term introduces an entropy increase across the mixing plane interface that exists between the stationary and rotating domains, and is introduced due to the assumptions of the numerical model.

The key aerodynamic performance metrics used in this study are the total-to-total efficiency (η_{tt}), stator loss coefficient (ξ_N), and rotor loss coefficient (ξ_R), which are given by Eqs. (1)–(3)

$$\eta_{tt} = \frac{(h_{01} - h_{03})}{(h_{01} - h_{03ss})} \tag{1}$$

$$\xi_N = \frac{(h_2 - h_{2s})}{\frac{1}{2}{C_2}^2} \tag{2}$$

$$\xi_R = \frac{(h_3 - h_{3s})}{\frac{1}{2}{V_3}^2} \tag{3}$$

where h_{01} is the total enthalpy at the nozzle inlet, h_{03} is the total enthalpy at the rotor outlet, h_{03ss} is the isentropic total enthalpy at the rotor outlet evaluated at the nozzle inlet entropy and the rotor outlet total pressure, h_2 is the static enthalpy at the nozzle outlet, h_{2s} is the isentropic static enthalpy at the nozzle outlet defined as a function of the nozzle inlet entropy and interface pressure, c_2 is the absolute velocity at the nozzle outlet, h_3 is the static enthalpy at the rotor outlet, h_{3s} is the isentropic static enthalpy at the rotor outlet defined as a function of the rotor inlet entropy and outlet pressure, and V_3 is the relative rotor velocity at the outlet. All velocity values are area averaged, while the enthalpy values are mass averaged.

Table 2 Definition of the four tested meshes

Grid	First layer thickness (mm)	Growth rate	Number of layers in the spanwise direction	Total number of grid points per passage (millions)
Grid 1	2.485	1.3	30	0.31
Grid 2	1.243	1.2	40	0.70
Grid 3	4.97×10^{-3}	1.15	40	1.40
Grid 4	2.49×10^{-3}	1.1	48	2.90

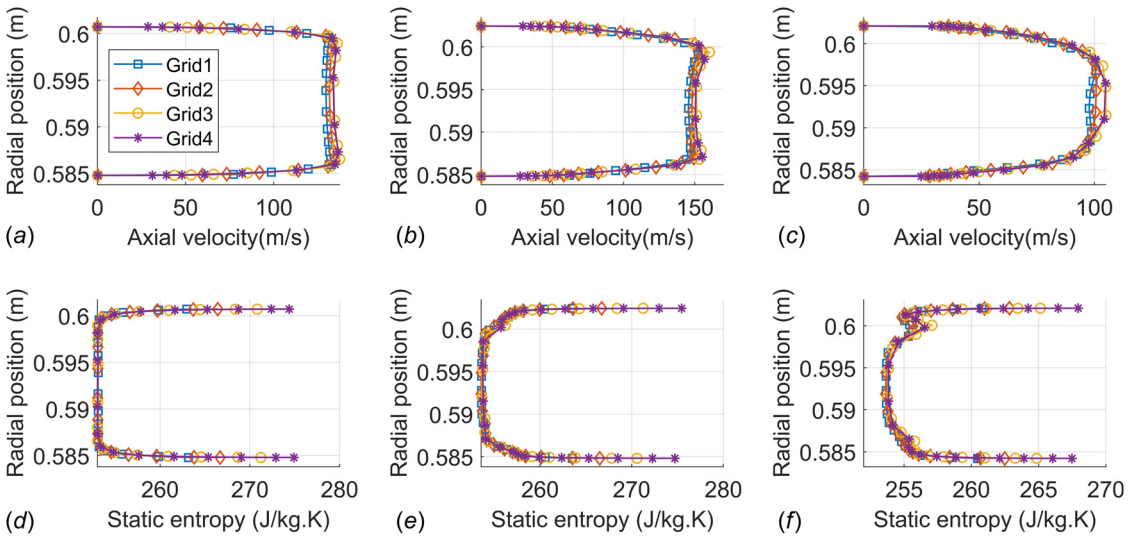

Fig. 4 Axial velocity and entropy radial distributions at different locations for different grid structures: (*a*) Velocity near the stator suction side, (*b*) velocity near the rotor suction side, (*c*) velocity downstream the rotor trailing edge, (*d*) entropy near the stator suction side, (*e*) entropy near the rotor suction side, and (*f*) entropy downstream the rotor trailing edge

2.1 Review of Loss Audit Approaches. To quantify aerodynamic losses using CFD simulations, different aerodynamic loss breakdown approaches have been previously published within the literature. In this section, four methods applying the sequential elimination approach are presented which include those conducted by Yoon et al. [14], De-Servi et al. [11], Wheeler and Ong [13], and Keep and Jahn [15], while the single model approach is reviewed based on the methodology presented by Denton and Pullan [18] and Newton et al. [19]. These methodologies are presented first, before the approach developed in the current work is introduced. Both the reviewed and the proposed methodologies are applied to a four-stage sCO_2-C_6F_6 turbine to verify the proposed methodology and to provide a better understanding of the conceptual differences between the methodologies.

Yoon et al. [14] proposed setting up a series of CFD simulations where loss sources are eliminated sequentially to estimate their magnitudes. First, a standard model is setup including all the loss sources to serve as the reference case for the analysis. Second, the effect of viscosity near the stator and rotor endwalls is removed by setting up free slip boundary condition on the hub/shroud walls, which allows endwall losses to be estimated. Following this, the viscous effects near the stator and rotor blades are eliminated to assess the effect of blade profile losses by setting up free slip boundary condition on the stator, and rotor blade walls. The final

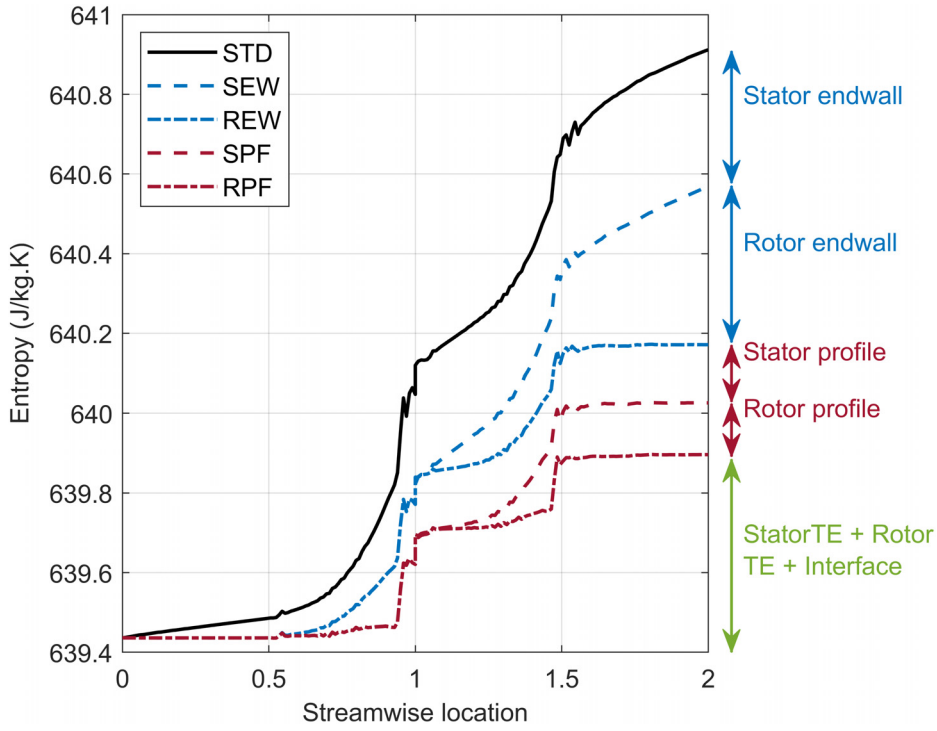

Fig. 5 Comparison of the entropy distribution along the normalized streamwise location of different CFD models following Yoon et al. [14] methodology applied to sCO_2-C_6F_6 turbine

model is thus expected to only include trailing edge and interface losses. Once the series of models have been developed, the performance of each model is assessed and the differences between the models are used to estimate the contribution of each source of loss individually.

The methodology presented by Yoon et al. has been applied to the sCO_2-C_6F_6 case study for the purpose of demonstrating the model, while further details about this case study are provided later in Sec. 4. The axial distribution of the mass averaged entropy from the stage inlet to the stage outlet is given in Fig. 5. The differences between the inlet and outlet entropy of each model give an indication of the effect of the removed source. In more detail, the difference between inlet and outlet entropy of the standard (STD) model and the model without stator endwall (SEW) provides the entropy generated due to the stator endwall. Similarly, the difference between inlet and outlet entropy of the SEW model and the model without the rotor endwall (REW) indicates the effect of the rotor endwall loss. Repeating the process enables the quantification of the entropy generated due to the stator profile (SPF), rotor profile (RPF), and finally, the stator and rotor trailing edge. Additionally, the interface losses are calculated from the last model without any viscous effect on the walls by calculating the entropy increase across the stator (STE), the rotor (RTE), and the interface between rotor and stator (INT).

De-Servi et al. [11] proposed setting up multiple CFD models to quantify different loss sources by eliminating one or more sources from each model. The strategy followed by De-Servi et al. is further illustrated in Table 3. In this approach, two CFD models were setup to break down the aerodynamic loss sources within an ORC radial turbine. The first model eliminates the effect of viscosity near the endwalls, such that the remaining sources of loss are blade profile and trailing edge losses (also called mixing loss), while the second model is the standard one with viscous effects at all the walls. To evaluate blade profile and trailing edge losses from the first model, an extra plane is selected at the trailing edge where the entropy rise between the inlet to the blade and this plane defines the profile loss. Similarly, the entropy rise from this plane to the blade outlet defines the blade trailing edge loss. The second model is used to calculate the endwall losses by calculating the increase in entropy due to the existence of viscous effects on the hub and shroud walls compared to the first model.

The strategy of loss breakdown estimation introduced by Wheeler and Ong [13] and Keep and Jahn [15] is similar to that implemented by De-Servi et al. [11], except no intermediate planes are defined for the purpose of separating the trailing edge and profile losses. The loss breakdown in this case is limited to separating endwall loss, while the profile and trailing edge losses are obtained as a whole.

On the other hand, Denton and Pullan [18] presented a loss breakdown methodology based on a single CFD model results. In this method, the fluid domain is divided into a set of predefined regions where each source of loss is expected to dominate. The entropy generated in each of the predefined domains is quantified to give an indication of the loss breakdown structure. Although this method considers the cross-interaction between different loss sources, it requires calibration for each case study to trace the actual location of the boundary layer which depends on many design parameters such as fluid type, mass flowrate, blade aspect ratio, and operating conditions.

Taking into account the theory behind the published loss breakdown methodologies, the loss breakdown can be obtained more accurately by considering the cross interaction between the loss sources while defining the loss regions interactively with the flow results. The strategies presented by Yoon et al. [14], De-Servi et al. [11], Wheeler and Ong [13], and Keep and Jahn [15] have been applied to the sCO_2-C_6F_6 axial turbine case study. These are then compared with the mean line design model and the new loss audit approach proposed in this paper which allows a comparison and verification of the new approach. The results from this comparison are presented in Sec. 4.2.

2.2 Proposed Loss Audit Approach. In the present study, a new method has been proposed to quantify the different sources of loss using a single CFD simulation. Within the proposed method, the entropy rise is monitored at different locations, which vary for each case study considering the boundary layer development and entropy distribution across the flow path. Initially, the CFD simulation is carried out to obtain the velocity and entropy results. Then, monitoring planes are placed within the solution domain of each blade at the inlet, outlet, and just before and after the trailing edge as reported in Fig. 6. The inlet and outlet planes are used to quantify the total entropy rise per blade row. Whilst two other planes are defined before and after the trailing edge of each blade row to be used for breaking down the losses as shown in Fig. 6. The blade pressure side (PS) and suction side (SS) are mentioned in the figure for both stator and rotor domains.

Planes 1 and 3 are specified before the trailing edge of the stator and rotor, respectively, and are used to evaluate the effects of blade profile, endwall, and secondary flow losses. Planes 2 and 4 are specified downstream of the trailing edge of the stator and rotor respectively to evaluate the effect of the trailing edge losses, alongside blade profile, endwall and secondary flow losses as indicated in Table 4. For the upstream planes (P1 and P3), their locations are fixed at the center of the trailing edge arc. For the downstream planes, (P2 and P4), their location is set at a distance downstream of the trailing edge that is equal to the trailing edge thickness. However, a sensitivity analysis is carried out to quantify the sensitivity of this assumption as presented in Sec. 4.3.

On each of the specified planes, multiple curves are defined to help quantify each type of loss separately as represented by the thick solid lines in Fig. 7, which considers plane 1 as an example. Each

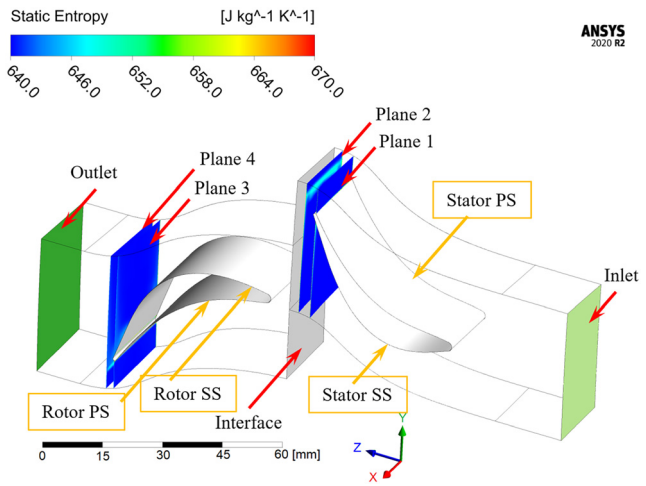

Fig. 6 Flow path division planes from inlet to outlet used for the developed methodology

Table 3 Loss breakdown strategy by De-Servi et al. [11]

Loss type	Averaging procedure	CFD model
Blade profile losses	Midspan: inlet boundary to TE	Free slip endwalls
Mixing loss	Midspan: TE to outlet boundary	Free slip endwalls
Endwall and secondary flow	Spanwise average: inlet to outlet	Standard model

Table 4 Details of monitoring planes assigned for loss breakdown analysis using the proposed methodology

Plane/streamwise location	Expected sources of loss
Stator inlet	None (stator reference)
P1: Just before the stator TE	Stator profile, stator endwall and stator secondary flows
P2: Midway between the stator TE and the interface	Total stator losses (profile, endwall, secondary flows and TE)
Stator outlet	Total stator losses
Rotor inlet	Total stator loss + interface losses (rotor reference)
P3: Just before the rotor TE	Rotor profile, rotor endwall and rotor secondary flows
P4: Downstream the rotor TE (4–6% of the chord length)	Total rotor losses (profile, endwall, secondary flows and TE)
Rotor outlet	Total rotor losses+ outlet domain losses

plane is divided into five contours; left, right, top, bottom, and middle contours, using the four bounding curves. The left and right domains represent the effect of hub and shroud walls (endwall losses); the middle domain represents the profile losses in planes 1 and 3, or the combined effect of the blade profile and trailing edge in planes 2 and 4; the remaining two planes (top and bottom) are assigned to secondary flows. The concept behind the selection of these contours relies on the definition of each type of loss. Endwall losses are formed within the hub/shroud boundary layers, the profile losses are developed within the blade wall boundary layers, the trailing edge losses are formed just downstream of the trailing edge and around it, while the secondary flow losses are considered within the rest of the flow passage.

Within the defined loss contour, the entropy rise is calculated relative to the reference entropy at the domain inlet to quantify the contribution of each source of loss. Considering the elements within each contour, the mass averaged entropy is calculated from Eq. (4). The mass flowrate through each contour is calculated from Eq. (5), while the mass flow average entropy rise for each contour is calculated from Eq. (6). It should be noted that the summation of the actual mass flow average entropy rise per contour results in the total entropy rise up to the selected plane as shown in Eq. (7)

$$s_i = \frac{\dot{m}_e s_e}{\sum(\dot{m}_e)} \tag{4}$$

$$\dot{m}_i = \sum(\dot{m}_e) \tag{5}$$

$$\Delta s_i = (s_i - s_{\text{in}})\frac{\dot{m}_i}{\dot{m}_n} \tag{6}$$

$$\Delta s_n = (s_n - s_{\text{in}}) = \sum(\Delta s_i) \tag{7}$$

In this set of equations, e represents the element value, i represents the contour, n represents the plane number, s_i is the mass flow average entropy of any contour, $\dot{m}_e$ is the mass flow per element, s_e is the elements entropy, $\dot{m}_i$ is the contour mass flowrate, Δs_i is the entropy rise for each contour, s_{in} is the inlet mass flow averaged entropy, $\dot{m}_n$ is the total mass flowrate per plane, Δs_n is the entropy rise over the entire plane relative to the inlet entropy, and s_n is the plane mass flow averaged entropy. The values of mass flowrate and entropy of the plane $\dot{m}_n$ and s_n can be calculated using the same contour equations (i.e., Eqs. (4) and (5)), considering the elements of the entire plane rather than the elements of each specific contour.

3 Verification Case Study

To our knowledge, for the sCO_2/C_6F_6 turbine, and for supercritical CO_2 in general, there is no experimental data available against which to experimentally validate the CFD model. This is particularly true for large scale axial turbines, which elevates the need for the numerical assessment of the design. In the absence of such data, the CFD model is verified against the available experimental data for a small-scale air turbine. The presented CFD model has also been verified against numerical results of a sCO_2 turbine available in the literature, as detailed in the author's previous publication [4]. The loss breakdown obtained via the proposed approach is also verified against the other published loss audit approaches for a 130 MW turbine operating with a CO_2/C_6F_6 blend.

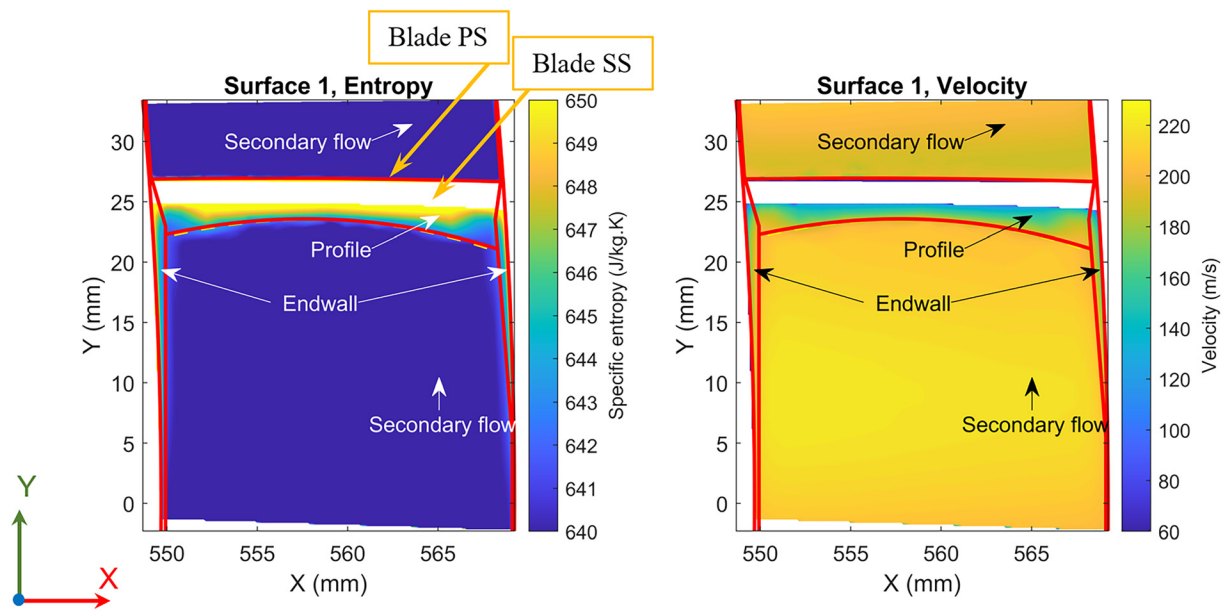

Fig. 7 Loss contours on plane 1, (left) entropy distribution, and (right) velocity magnitude distribution

Table 5 Air turbine case study definition [25]

Parameter	Value
Working fluid	Air
Inlet total pressure (bar)	1.25
Inlet total temperature (K)	358
Inlet turbulence intensity	5% (medium)
Outlet static pressure (bar)	0.98
Hub, shroud, and blade walls	Adiabatic, smooth
Rotational speed (RPM)	7200

In the first verification study, a small-scale air turbine has been selected due to the similarity between an air turbine and a turbine operating with a sCO_2 blend in that both will operate in the subsonic regime. However, laminar flow is expected to occur for the small-scale air turbine, whilst the turbine operating with sCO_2 is expected to operate in the turbulent flow regime.

The selected case study is a single-stage axial air turbine rated at 140-kW where numerical and mean line results were published by Meroni et al. [25] and compared to experimental results published by Evers and Kötzing [26]. The boundary and operating conditions are presented in Table 5.

Two designs are generated using the mean line design tool based on the Aungier loss model, and these correspond to designs with and without tip clearance. The design with tip clearance is used to validate the performance predictions obtained from the mean line design and CFD models against experimental data, which includes the overall total-to-total efficiency as well as the stator and rotor enthalpy loss coefficients. The later design, without tip clearance, is considered to enable a comparison between the loss breakdown predicted by the mean line loss model and the new loss audit approach. This is required to verify the breakdown obtained using the numerical model against the mean line loss model. The differences between mean line model, CFD model and experimental results are summarized in Table 6.

The results obtained via both CFD and the mean line design model for the total-to-total efficiency show a good agreement with the experimental results [27,28], although a larger error is observed for the mean line model compared to the CFD. It is also noted that the mean line loss model overestimates the stator loss coefficient and underestimates the rotor loss coefficient, with a higher deviation in the stator loss coefficient of 74.1% of the experimental value compared to 18.4% for the rotor loss coefficient. This error is almost the same error as that obtained by Meroni et al. [25] when they compared their mean line model results to the experimental results where the error in the stator loss coefficient was around 72%.

The error in the CFD model is significantly lower with a deviation of 5.0% and 1.7% for the stator and rotor loss coefficients, respectively. The differences in the total-to-total efficiency reflect the differences in the loss coefficients, as the relative error in the mean line model is 1.6% compared to 0.9% for the CFD. By comparing the mean line design and CFD results for the case with tip clearance, it can be noted that the largest deviation is recorded for the stator loss coefficient whilst the smallest difference is found for the efficiency.

The second model without tip clearance shows similar trends, where similar differences to the tip clearance model are observed for the stator loss coefficient, which is overestimated using the mean line model. For the rotor loss coefficient, a smaller difference is found, where the mean line loss model underestimates the rotor losses, while overall it calculates a slightly higher total-to-total efficiency. These differences can be further investigated by comparing the loss breakdown obtained from the mean line and CFD models.

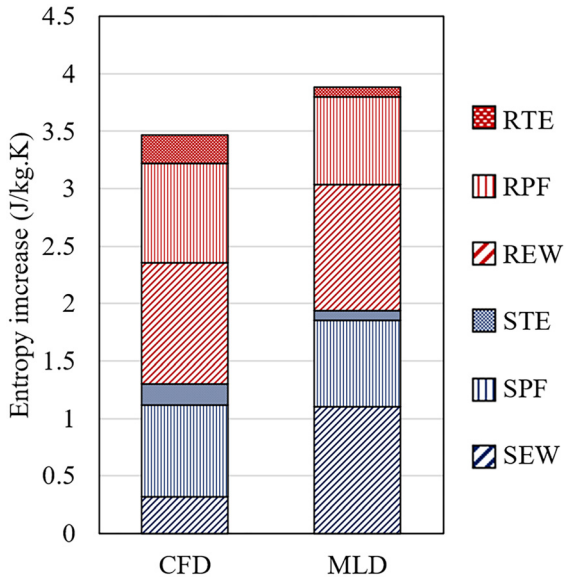

Fig. 8 Loss breakdown structure of the air turbine case study

The loss breakdown of the turbine design without tip clearance has been assessed using the proposed CFD approach and compared to the mean line loss model in Fig. 8. It can be seen from the results that the stator endwall loss is significantly larger in the mean line model, which helps explain the differences found in Table 6 for the two models with and without tip clearance. The rotor losses predicted by the mean line model are slightly lower compared to the CFD model, with the rotor profile and rotor trailing edge accounting for the largest differences. Overall, the loss breakdown is in good agreement, except for the stator endwall loss. It is worth noting that the mean line loss models implement the same definitions for estimating the endwall loss within both the stator and rotor. However, it is expected that the endwall losses within the stator blades should be smaller compared to the rotor blades. This is because the turbulence intensity in the stator domain is affected by the turbulence intensity at the stage inlet, while the rotor is affected by the turbulence generated in the stator domain that is transferred through the interface to the rotor and results in significantly higher turbulence intensity.

The proposed approach for assessing the loss breakdown using CFD was further verified against other loss audit techniques from the literature [11,13–15], and applied to a turbine design 4-stages CO_2/C_6F_6 mixture. The results of the different CFD approaches have shown a good agreement, and these are further discussed in Sec. 4.2.

4 Results and Discussions

In the present study, the loss breakdown methodology is applied to a 130 MW four-stage axial turbine operating with CO_2/C_6F_6. The

Table 6 Overall performance verification of the air turbine case study

		With tip clearance = 0.24 (mm)					Without tip clearance		
Parameter	Exp. data [27,28]	MLD	CFD	Error MLD	Error CFD	CFD-MLD Deviation	MLD	CFD	CFD-MLD Deviation
ζ_N	0.0379	0.066	0.0398	74.1%	5.0%	−39.7%	0.0662	0.0365	−44.9%
ζ_R	0.0908	0.0741	0.0893	−18.4%	−1.7%	20.5%	0.0549	0.0676	23.1%
η_{tt} (%)	91.6%	93.1%	92.5%	1.6%	0.9%	−0.7%	94.0%	93.2%	−0.8%

Table 7 Mean line design geometry of the first and last stages of the sCO_2-C_6F_6 4-stage turbine

Parameter	S_{first}	R_{first}	S_{last}	R_{last}
Axial chord (mm)	38.5	40.6	39.3	41.3
Hub radius (mm)	549.7	549.7	549.7	549.7
Inlet tip radius (mm)	567.7	569.7	587.2	590.2
Outlet tip radius (mm)	569.3	572.1	589.4	595.7
Number of blades	100	95	100	95
Inlet blade angle (deg)	0.0	0.0	0.4	−2.5
Outlet blade angle (deg)	64.1	65.2	64.0	65.3
Stagger angle (deg)	34.7	34.8	34.5	35.2
Outlet fillet radius (mm)	0.8	0.8	0.8	0.8
Throat opening (mm)	15.7	16.6	16.1	16.7

Table 8 Boundary and operating conditions of the sCO_2-C_6F_6 turbine model

Parameter	Value
Blend	sCO_2/C_6F_6
Molar fraction (%)	16.7
Inlet total pressure (bar)	250
Inlet total temperature (K)	973.15
Outlet static pressure (bar)	77
Rotational speed (RPM)	3000
Power (MW)	130
Mass flow rate (kg/s)	1054
Number of stages	4
Stage pressure ratio	1.28

loss breakdown is obtained for the first and last stages that represent the maximum and minimum pressure levels, respectively, to understand the effect that changes in the density and viscosity of fluid may have on the loss structure. The developed methodology is then compared against other published loss audit approaches from the literature for the same case study.

The operating conditions for the proposed turbine model are reported in Table 8 while the one-dimensional blade geometries of the first and last turbine stages are summarized in Table 7. It is worth mentioning that some geometrical parameters that are required to construct the 3D blade are not obtained within the mean line (one-dimensional) analysis. This includes the blade inlet fillet radius, inlet/outlet wedge angles, the control points for the pressure and suction sides of the blade, twist angle, and the circumferential/axial lean angles. Hence, these shape parameters are set based on manual iterations that aim to achieve a smooth flow through the turbine with minimal secondary flows while matching the mass flowrate obtained using the 3D numerical simulation to the design mass flowrate for the given pressure ratio. The 3D blade is constructed by extruding the blade profile in the spanwise direction and as such the blade angles do not vary significantly along the blade height. This approach is considered suitable since the blade height is small compared to the hub diameter, and therefore, significant changes in the flow angles in the spanwise direction brought about by the change in tangential velocity are not expected.

Prior to the loss breakdown comparison, the mean line design is compared against the CFD simulations for the first stage, and the results are provided in Table 9. The total deviation in the mass flowrate and power is found to be approximately 2.4% and 4.5%, respectively. In terms of performance, the stator loss coefficient, rotor loss coefficient, and total-to-total efficiency are compared, and a good agreement is noted in the total-to-total efficiency. However, relatively large differences are observed in loss coefficients which are discussed under the detailed loss breakdown results. It can, however, be noted that the deviation in the stator loss coefficient is significantly larger than the rotor loss coefficient, which is similar to the findings for the air-case study, as previously described in Sec. 3.

Table 9 Mean line and CFD results for the first stage of the 130 MW sCO_2-C_6F_6 turbine

Parameter	CFD	MLD	Difference
Mass flow rate (kg/s)	1080	1054	−2.40%
Power (MW)	35.5	33.9	−4.50%
η_{tt} (%)	94.52	93.10	−1.50%
ζ_N	0.0419	0.0604	44.10%
ζ_R	0.0562	0.059	5.00%

4.1 Loss Breakdown Using the Developed Methodology. The loss breakdown of the CO_2/C_6F_6 case study is obtained using the methodology discussed in Sec. 2.2 by defining the contours of different loss sources on each plane according to the loss definitions. The absolute velocity magnitude is used to define the contours defined on the different planes, whilst entropy values for the different contours are estimated to obtain the loss breakdown. Loss sources are defined using the contours as indicated in Fig. 9. The values for each loss source at the different planes, expressed as percentage of the total loss, and the corresponding increases in entropy are summarized in Table 10.

The entropy rise distributions calculated for each of the monitoring planes, as reported in Table 10, are used to calculate the detailed loss breakdown for each blade row (i.e., stator or rotor). For the stator, planes 1 and 2 are used to calculate the stator endwall, stator profile and stator trailing edge losses. The stator endwall losses are calculated from the endwall region of the downstream plane (P2), which accounts for the entropy increase across the whole stator domain. Similarly, the secondary flow losses are extracted from P2 while the profile losses are calculated from the upstream plane (P1) since it does not account for the trailing edge effect. The trailing edge losses can be calculated from the difference between the profile and trailing edge contributions in P2 and the profile contribution of P1. These calculations are repeated using P3 and P4 to obtain the loss breakdown of the rotor domain. The results of the detailed loss breakdown are reported for the first and last turbine stages in Table 11, in addition to the summation of losses per blade row, and per type of loss. This is done to provide an overall evaluation of the dominant loss sources and loss regions. In Table 11, the total losses per blade row are the summation of the endwall, secondary flow, profile and trailing edge losses for the stator and rotor individually. The stator–rotor interface losses are calculated from the CFD model as the difference in entropy across the two sides of the interface. The total losses per source are obtained by summing up the same loss types within both the stator and rotor losses, noting that the endwall losses include both endwall and secondary flow losses. The percentages given in the table represent the ratio between each loss type to the total losses. For example, the total endwall source percentage is the ratio between the endwall losses to the summation of endwall, profile and trailing edge losses.

The endwall and profile losses are found quite similar in the first stage, contributing to 39.5% and 38.2% for the endwall and profile, respectively, of the total stage losses. Similarly, the endwall and profile losses for the last turbine stage are found to be 34.6% and 33.7%, respectively, as indicated in Table 11. It can be inferred that rotor losses are large in both stages, and more specifically are almost 1.5 times the stator losses. This is reasonable due to the higher turbulence experienced within the rotor blade row due to rotation and the high secondary flows within the rotating outlet domain. The least dominating loss source in both turbine stages is the trailing edge loss, which represents around 14.9% and 24.83% for the first and last stages of the total stage losses, respectively.

The loss breakdown of the first and last turbine stages is visually represented in Fig. 10(*a*). The secondary flow and endwall losses are combined and named endwall losses to allow for easy comparison with other studies from the literature. However, the detailed breakdown is reported in Fig. 10(*b*) to provide a thorough investigation of the reasons behind performance deterioration, and hence better conclusions can be drawn to identify the dominating

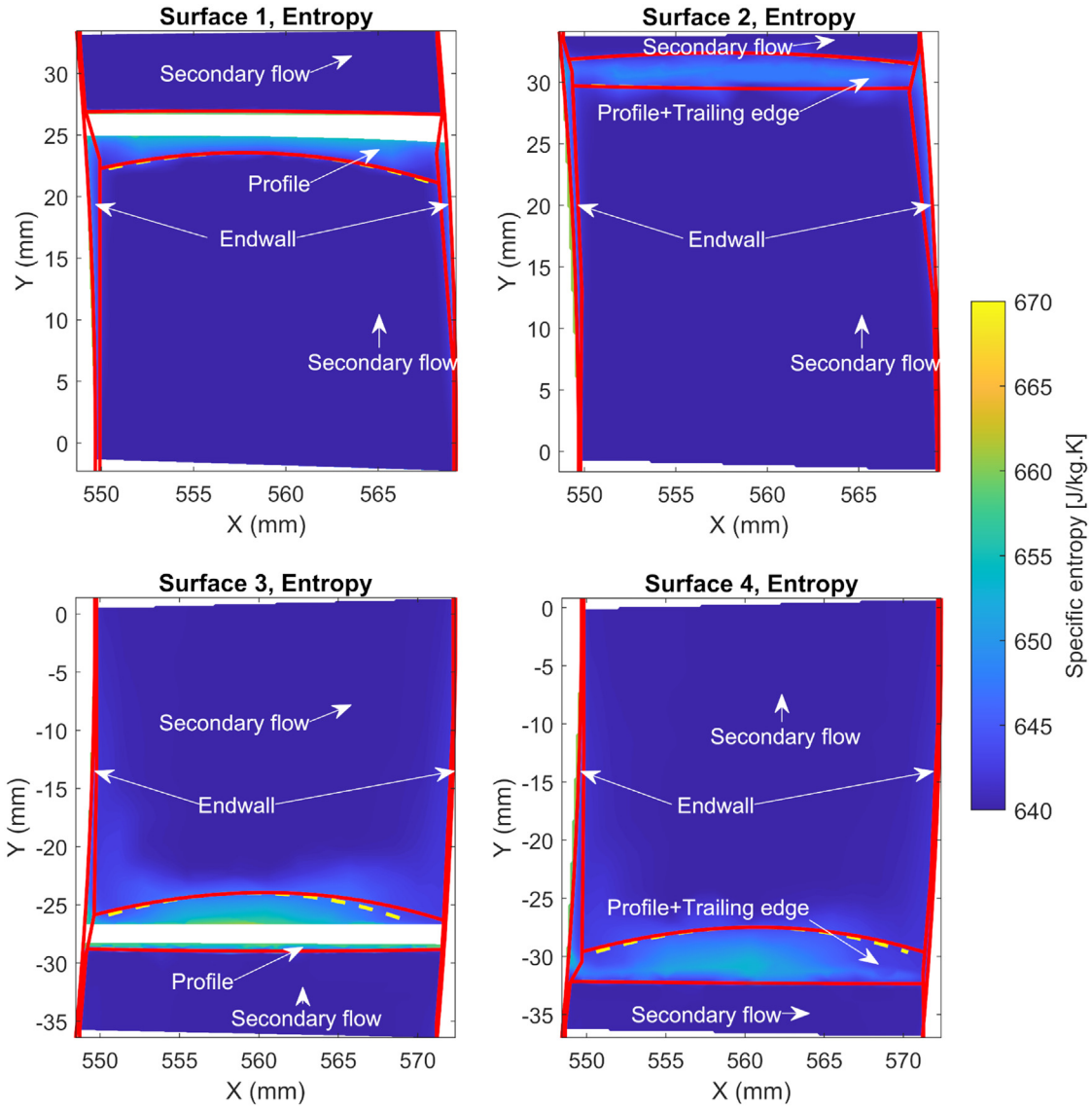

Fig. 9 Loss contours plotted over the entropy distribution on the selected monitoring planes 1:4

Table 10 Percentages of different sources of loss at each plane, first stage of the sCO_2-C_6F_6 design

Domain	Cut plane	Contour type	Δs (J/kg K)	Percentage of the total Δs
Stator	Plane 1	Total entropy rise	0.508	
		Endwall	0.087	17.1%
		Profile	0.286	56.4%
		Secondary flow	0.135	26.5%
	Plane 2	Total entropy rise	0.611	
		Endwall	0.104	16.9%
		Profile + trailing edge	0.323	52.7%
		Secondary flow	0.185	30.3%
Rotor	Plane 3	Total entropy rise	0.536	
		Endwall	0.026	4.8%
		Profile	0.313	58.3%
		Secondary flow	0.197	36.9%
	Plane 4	Total entropy rise	0.631	
		Endwall	0.042	6.7%
		Profile + trailing edge	0.510	80.8%
		Secondary flow	0.079	12.5%

Table 11 Results of the detailed loss breakdown for the first and last stages of the sCO_2-C_6F_6 design

Type	Source	First stage		Last stage	
		Δs (J/kg K)	%	Δs (J/kg K)	%
Break down	Stator endwall	0.10	6.6%	0.05	3.55%
	Stator secondary flow	0.19	11.8%	0.12	7.80%
	Stator profile	0.29	18.3%	0.23	15.52%
	Stator trailing edge	0.04	2.3%	0.14	9.55%
	Stator-rotor interface	0.12	7.4%	0.10	6.83%
	Rotor endwall	0.04	2.7%	0.03	2.03%
	Rotor secondary flow	0.08	5.0%	0.13	9.04%
	Rotor outlet domain	0.21	13.3%	0.18	12.19%
	Rotor profile	0.31	20.0%	0.27	18.20%
	Rotor trailing edge	0.20	12.6%	0.23	15.28%
Total per blade row	Stator	0.61	39.0%	0.538	36.42%
	Rotor	0.84	53.6%	0.839	56.75%
	Stator-rotor interface	0.12	7.4%	0.101	6.83%
Total per source	Endwall losses	0.62	39.5%	0.512	34.62%
	Profile losses	0.60	38.2%	0.499	33.72%
	Trailing edge losses	0.23	14.9%	0.367	24.83%

sources of loss. Higher stage losses are obtained in the first stage compared to the last stage as indicated in Fig. 10. This is due to the significant reduction in endwall losses in the last stage compared to the first stage for both the rotor and stator, although both stages experience similar profile and trailing edge losses.

The turbine is designed assuming repeating stages, and therefore the absolute velocity at the stage inlet is the same for each stage. Due to the reducing pressure and density, this leads to longer blades in the downstream stages where the relative contribution of the endwall losses is reduced due to the smaller relative endwall boundary layer thicknesses compared to the blade height. By looking at the detailed breakdown (i.e., Fig. 10(*b*)), it can be observed that the endwall losses are reduced when moving from the first stage to the last. However, secondary flow losses are observed to increase due to the increased turbulence intensity away from the walls. Furthermore, it is observed that the blade profile losses decrease, which means that the flow streamlines are better aligned with the blades within the last stage compared to the first stage.

4.2 Comparisons of Loss Breakdown Approaches. In this section, the different loss breakdown approaches from the literature are compared to the proposed approach to verify the new approach and investigate the effect of the interaction between the different loss sources on the loss structure.

By analyzing the loss breakdown obtained by the various approaches based on multiple CFD models, it is evident that De-Servi et al., Wheeler and Ong, and Keep and Jahn approaches calculate the same endwall loss. Nonetheless, Wheeler and Ong and Keep and Jahn predict higher profile losses compared to the other two approaches due to combining the effect of both profile and trailing edge losses as indicated in Fig. 11. As a whole, the total stator and rotor losses are the same for De-Servi et al., Wheeler and Ong and Keep and Jahn; however, De-Servi et al. do not account for interface losses so that stage efficiency increases since the losses are reduced. The loss breakdown estimated using the approach adopted by Yoon et al. agrees with the other approaches from the literature although trailing edge losses in this approach are overestimated compared to the other two approaches. This is due to calculating the trailing edge losses from the CFD model without viscous effects near the walls; instead, the total entropy rise in the rotor and stator rows are considered only due to trailing edge losses, neglecting the effects of secondary flow losses and vortices.

Compared to the published multiple model approaches, the proposed approach in the current study predicts lower endwall losses

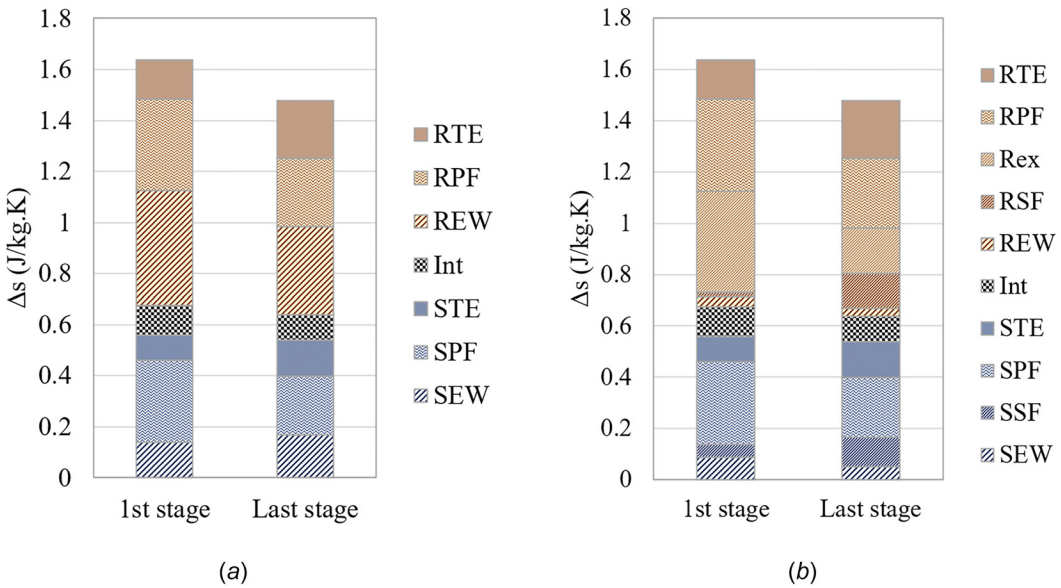

Fig. 10 Loss breakdown of the first and last turbine stages: (*a*) summarized and (*b*) detailed

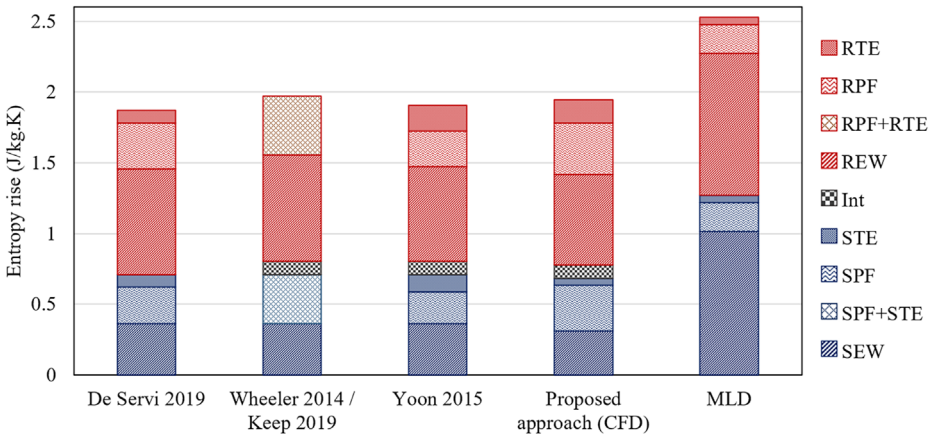

Fig. 11 Comparison between different loss breakdown approaches applied to the first stage of the sCO_2-C_6F_6 four-stage design

in both rotor and stator blades. That is expected since, in the multiple-model approaches, the elimination of the endwall source affects other types of losses such as profile and trailing edge losses by decreasing the turbulence kinetic energy in the subsequent CFD model of the series. As a result, the elimination approaches overestimate the endwall losses and underestimate the other sources of loss. Specifically, the stator and rotor endwall losses are on average overestimated by 16% and 13%, respectively, compared to De-Servi et al., Wheeler and Ong, Keep and Jahn, and Yoon et al. approaches. The stator and rotor profile losses are under estimated by 19% and 11%, respectively, compared to De-Servi et al. and by 29% and 31% compared to Yoon et al.

Although some differences in the trailing edge losses are obtained between the proposed approach and the published approaches, those differences are not considered significant since this type of loss does not have a dominant effect on the stage performance. Specifically, the contribution of the trailing edge loss to the total stage losses is between 10% and 15%. It can be noted that the stator trailing edge loss evaluated using the proposed approach is less than all the published approaches, while the rotor trailing edge loss is close to that of Yoon et al. and larger than De-Servi et al. Finally, the interface losses are the same as the other approaches that account for it, representing around 5% of the total stage loss.

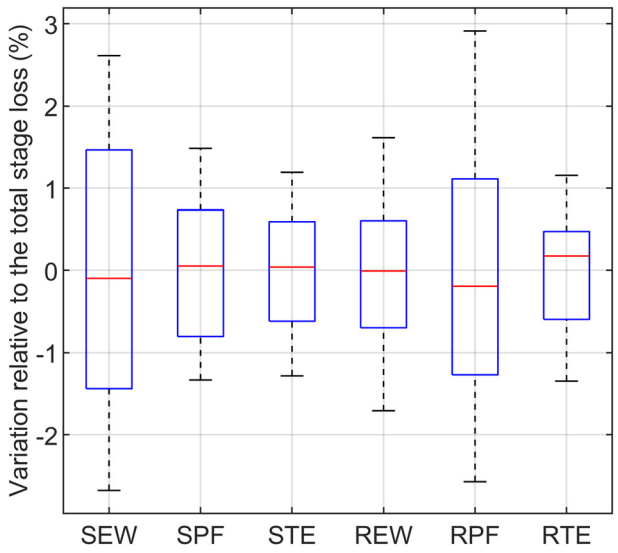

Fig. 12 Sensitivity of the loss breakdown structure to contours selection process obtained by repeating the selection 10-times for the same case study

Despite the differences between the proposed approach and the previously reported approaches, it is worth noting that a good agreement is obtained for the overall performance. Furthermore, the loss breakdown results obtained using CFD results, using the different approaches, have been compared to the predictions from the mean line design that utilizes the Aungier loss model [7]. In contrast to the comparison between the loss audit approaches, larger differences are observed with endwall and profile losses being overestimated, and the trailing edge losses being underestimated compared to the CFD models. The values for the stator and rotor endwall losses calculated using the mean line loss model are found to be approximately 3.2 and 1.6 times the CFD values, respectively. The profile losses are underestimated by the mean line model, with values for the stator and rotor that are 64% and 56% lower than the CFD values, respectively.

The rotor trailing edge loss calculated using the CFD model is three times higher than the mean line prediction. In the CFD model, the boundary layer that develops along the blade walls contributes to the trailing edge loss calculation. As such, both the profile and trailing edge losses will increase if the flow becomes more turbulent within the rotor domain due to blades rotation or flow angles deviation from the blade angles.

4.3 Sensitivity Analysis. The sensitivity of the loss breakdown results to the position of the contours used to define the different loss regions is evaluated by shifting the contour lines of the same model and the same monitoring planes. A set of cases are defined by shifting the endwall contours in the radial direction by $\pm 1\%$ of the blade height and the profile contours in the circumferential direction by $\pm 20\%$ of the blade trailing edge thickness. Each variable is divided into 10 steps to produce a test sample of 100 cases. The range of entropy rise variation calculated for each loss type, relative to the total entropy rise across the stage, is presented in Fig. 12. In this figure, the box represents the range for 50% of the test sample, the horizontal partitioning line indicates the median and the dashed outside lines indicate the minimum and maximum values. It can be noted that the obtained loss breakdown results are not that sensitive to the contour selection process as most of the variations are less than 2% of the total losses. The highest variation is calculated for the stator endwall with a range of 5%, while the lowest variations are found for the rotor and stator trailing edge losses with a range of around 2.5%. The small variations of the trailing edge losses are due to their relatively small values compared to the total stage losses

The sensitivity of the loss breakdown to the monitoring plane location downstream of the stator and rotor blades trailing edge is presented in Fig. 13. This analysis is conducted by changing the location of plane 2 and plane 4 by $\pm 20\%$ relative to the axial gap between the blade trailing edge and the domain outlet. These planes affect the endwall and trailing edge losses while the profile and

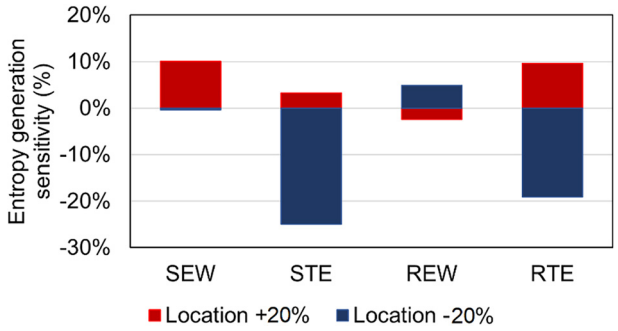

Fig. 13 Sensitivity of loss breakdown structure to the planes location (P2 and P4)

interface losses are independent of the location of the selected planes. For planes 1 and 3, the location is fixed at the center point of the trailing edge arc. The results are summarized in Fig. 13. Endwall losses are found to be insensitive to the selected plane location with a maximum uncertainty of 10% for the stator endwall and 5% for the rotor endwall. The trailing edge losses are found more sensitive to the plane's location with a maximum uncertainty of 25% and 18% for the stator and rotor, respectively. Despite this high sensitivity, it is worth noting that this sensitivity is not significant in the conducted analysis due to the small contribution of the trailing edge losses to the total loss breakdown as illustrated in Fig. 12.

5 Conclusions

In this paper, an improved loss breakdown estimation approach using CFD results is presented that is suitable for accurate predictions in compact turbines that use nonconventional working fluids such as sCO_2 and sCO_2 blends. Different loss estimation approaches from the literature were investigated and compared to the developed methodology. The approach proposed in this paper addresses shortcomings of the previously published approaches by considering the interaction between different loss sources in addition to considering the variation in boundary layer thickness between different case studies. This is considered important for dense working fluids such as pure CO_2 and CO_2 blends.

The proposed model was verified against experimental and numerical data for a 140 kW air turbine. The results showed good agreement between the CFD model and the experimental data with deviation in the total-to-total efficiency, stator loss coefficient, and rotor loss coefficient of 0.9%, 5.0%, and −1.7%, respectively. The proposed loss breakdown approach was verified by comparing the results to the other published approaches, where a good agreement was obtained. However, some differences were captured that are related to how each loss audit approach is conducted.

By comparing the results obtained using the previously published approaches to the proposed approach, it was found that the proposed approach predicts lower endwall losses in both the rotor and stator domains. This is because eliminating endwall viscous effects from the model, as done in the previous approaches, decreases the other loss sources since the cross-interaction between different loss sources is removed. Therefore, the results using the elimination-based approach tend to overestimate the endwall losses and underestimate the other sources of loss.

A sensitivity study was carried out to evaluate the uncertainty of the proposed approach in response to definition of the planes and contours which are defined to carry out the loss audit. The results have shown the endwall and profile losses have a low sensitivity to these parameters, where the sensitivity to the contour and plane location was less than 21% and 10%, respectively. However, a higher sensitivity was observed for the trailing edge losses, although trailing edge losses themselves were not found to be a dominant source of loss. Specifically, the sensitivity of the trailing edge losses to the selected contour and plane location was found to be 70% and 23%, respectively.

Funding Data

- European Union's Horizon 2020 Research and Innovation Programme (Grant No. 814985; Funder ID: 10.13039/100010661).

Nomenclature

C = absolute velocity magnitude (m/s)
h = enthalpy (J/kg)
M = Mach number
$\dot{m}$ = mass flow rate (kg/s)
s = entropy (J/kg.K)
T = temperature (K)
V = relative velocity magnitude (m/s)

Abbreviations

INT = interface
MLD = mean line design
NGV = nozzle guide vanes
REW = rotor endwall
RPF = rotor profile
RSF = rotor secondary flow
RTE = rotor trailing edge
SEW = stator endwall
SPF = stator profile
SSF = stator secondary flow
STD = standard
STE = stator trailing edge

Greek Symbols

η_{tt} = total to total efficiency
ζ = enthalpy loss coefficient

Subscripts

01 = stator inlet, total condition
1 = stator inlet
2 = stator-rotor interface
2s = isentropic state at stator outlet
03 = rotor outlet, total condition
3 = rotor outlet
3s = isentropic state at rotor outlet relative to rotor inlet entropy
03ss = isentropic state at rotor outlet relative to stator inlet entropy, total condition
e = element number
i = contour number
n = Plane number
N = nozzle/stator
P = profile
R = rotor
tc = tip clearance
TE = trailing edge

References

[1] White, M. T., Bianchi, G., Chai, L., Tassou, S. A., and Sayma, A. I., 2021, "Review of Supercritical CO_2 Technologies and Systems for Power Generation," Appl. Therm. Eng., **185**, p. 116447.
[2] Turchi, C. S., Ma, Z., Neises, T. W., and Wagner, M. J., 2013, "Thermodynamic Study of Advanced Supercritical Carbon Dioxide Power Cycles for Concentrating Solar Power Systems," ASME J. Sol. Energy Eng., **135**(4), p. 041007.
[3] Luo, D., Liu, Y., Sun, X., and Huang, D., 2017, "The Design and Analysis of Supercritical Carbon Dioxide Centrifugal Turbine," Appl. Therm. Eng., **127**, pp. 527–535.
[4] Abdeldayem, A., White, M., Paggini, A., Ruggiero, M., and Sayma, A. I., 2022, "Integrated Aerodynamic and Structural Blade Shape Optimisation of Axial Turbines Operating With Supercritical Carbon Dioxide Blended With Dopants," ASME J. Eng. Gas Turbines Power, **144**(10), p. 101016.
[5] Dunham, J., and Came, P., 1970, "Improvements to the Ainley-Mathieson Method of Turbine Performance Prediction," ASME J. Eng. Power, **92**(3), pp. 252–256.
[6] Kacker, S., and Okapuu, U., 1982, "A Mean Line Prediction Method for Axial Flow Turbine Efficiency," ASME J. Eng. Power, **104**(1), pp. 111–119.
[7] Aungier, R. H., 2006, Turbine Aerodynamics, ASME, New York, pp. 61–92.

[8] Craig, H., and Cox, H., 1970, "Performance Estimation of Axial Flow Turbines," Proc. Inst. Mech. Eng., **185**(1), pp. 407–424.
[9] Langston, L., 2006, "Secondary Flows in Axial Turbines—A Review," Ann. New York Acad. Sci., **934**(1), pp. 11–26.
[10] Jang, H. J., Kang, S. Y., Lee, J. J., Kim, T. S., and Park, S. J., 2015, "Performance Analysis of a Multi-Stage Ultra-Supercritical Steam Turbine Using Computational Fluid Dynamics," Appl. Therm. Eng., **87**, pp. 352–361.
[11] De Servi, C. M., Burigana, M., Pini, M., and Colonna, P., 2019, "Design Method and Performance Prediction for Radial-Inflow Turbines of High-Temperature Mini-Organic Rankine Cycle Power Systems," ASME J. Eng. Gas Turbine Power, **141**(9), p. 091021.
[12] Denton, J., and Xu, L., 1990, "The Trailing Edge Loss of Transonic Turbine Blades," ASME J. Turbomach., **112**(2), pp. 277–285.
[13] Wheeler, A. P., and Ong, J., "A Study of the Three-Dimensional Unsteady Real-Gas Flows Within a Transonic ORC Turbine," ASME Paper No. V03BT26A003.
[14] Yoon, S., Vandeputte, T., Mistry, H., Ong, J., and Stein, A., 2016, "Loss Audit of a Turbine Stage," ASME J. Turbomach., **138**(5), p. 051004.
[15] Keep, J. A., and Jahn, I. H., 2019, "Numerical Loss Investigation of a Small Scale, Low Specific Speed Supercritical CO_2 Radial Inflow Turbine," ASME J. Eng. Gas Turbines Power, **141**(9), p. 091003.
[16] Pullan, G., Denton, J., and Curtis, E., 2006, "Improving the Performance of a Turbine With Low Aspect Ratio Stators by Aft-Loading," ASME J. Turbomach., **128**(3), pp. 492–499.
[17] Newton, P., Copeland, C., Martinez-Botas, R., and Seiler, M., 2012, "An Audit of Aerodynamic Loss in a Double Entry Turbine Under Full and Partial Admission," Int. J. Heat Fluid Flow, **33**(1), pp. 70–80.
[18] Denton, J., and Pullan, G., 2012, "A Numerical Investigation Into the Sources of Endwall Loss in Axial Flow Turbines," Proceedings of Turbo Expo: Power for Land, Sea, and Air, Copenhagen, Denmark, June 11–15, pp. 1417–1430.
[19] Newton, P., Martinez-Botas, R., and Seiler, M., 2015, "A Three-Dimensional Computational Study of Pulsating Flow Inside a Double Entry Turbine," ASME J. Turbomach., **137**(3), p. 031001.
[20] Salah, S. I., White, M. T., and Sayma, A. I., 2022, "A Comparison of Axial Turbine Loss Models for Air, sCO_2 and ORC Turbines Across a Range of Scales," Int. J. Thermofluids, **15**, p. 100156.
[21] Salah, S. I., Khader, M. A., White, M. T., and Sayma, A. I., 2020, "Mean-Line Design of a Supercritical CO_2 Micro Axial Turbine," Appl. Sci., **10**(15), p. 5069.
[22] Mangani, L., Casartelli, E., Hanimann, L., Wild, M., and Spyrou, N., 2014, "Assessment of an Implicit Mixing Plane Approach for Pump-Turbine Applications," IOP Conference Series: Earth and Environmental Science, **22**(2), p. 022003.
[23] Smirnov, P. E., and Menter, F. R., 2009, "Sensitization of the SST Turbulence Model to Rotation and Curvature by Applying the Spalart–Shur Correction Term," ASME J. Turbomach., **131**(4), p. 041010.
[24] Aqel, O., White, M., and Sayma, A., 2021, "Binary Interaction Uncertainty in the Optimisation of a Transcritical Cycle: Consequences on Cycle and Turbine Design," Proceedings of 4th European sCO_2 Conference for Energy Systems, Online, Mar. 23–24, pp. 164–176.
[25] Meroni, A., La Seta, A., Andreasen, J. G., Pierobon, L., Persico, G., and Haglind, F., 2016, "Combined Turbine and Cycle Optimization for Organic Rankine Cycle Power Systems—Part A: Turbine Model," Energies, **9**(5), p. 313.
[26] Evers, B., and Kötzing, P., 1990, "Test Case e/tu-4 4-Stage Low Speed Turbine," Test Cases for Computation Internal Flows Aero Engine Components, pp. 365–375, Report No. AGARD-AR-275.
[27] Groschup, G., 1977, Strömungstechnische Untersuchung einer Axialturbinenstufe im Vergleich Zum Verhalten Der Ebenen Gitter Ihrer Beschaufelung.
[28] Propulsion, A., and Panel, E., 1976, "Through-Flow Calculations in Axial Turbomachinery," Report No. AGARD-CP-195.